HEAT TRANSFER ENHANCEMENT IN THE COMPLEX GEOMETRIES FILLED WITH POROUS MEDIA

by

Zeinab Z. RASHED[a], Sameh E. AHMED[b,c], and Abdelraheem M. ALY[b,c*]

[a] Mathematics Department, Faculty of Science and Arts, Jouf University, Qurayyat, Saudi Arabia
[b] Department of Mathematics, Faculty of Science, King Khalid University, Abha, Saudi Arabia
[c] Department of Mathematics, Faculty of Science, South Valley University, Qena, Egypt

Original scientific paper
https://doi.org/10.2298/TSCI181218166R

The present numerical investigation aims to analysis the enhancement heat transfer in the nanofluid filled-complex geometries saturated with a partially layered porous medium. The vertical walls of the cavity are taken as complex wavy geometries. The horizontal walls of the cavity are flat with insulated temperature. The complex wavy cavity is filled with a nanofluid and the upper half of the wavy cavity is saturated with the porous medium. In the analysis, the governing equations are formulated for natural convection under the Boussinesq approximation in various environments including pure-fluid, nanofluid, and porous medium. In this investigation, the effects of the R*ayleigh number ($10^3 \le Ra \le 10^5$), Darcy parameter ($10^{-6} \le Da \le 10^{-3}$), thermophoresis parameter ($0.1 \le Nt \le 0.5$), nanofluid buoyancy ratio ($0.1 \le Nr \le 0.5$), Brownian motion parameter ($0.1 \le Nb \le 0.5$), inclination angle ($0° \le \gamma \le 90°$), and geometry parameters α_1 and R have been studied on the streamlines, temperature, nanoparticles volume fraction, local Nusselt number, and the local Sherwood number. It is found that, the performance of the heat transfer can be improved by adjusting the geometry parameters of the wavy surface. Overall, the results showed that the nanofluid parameters enhance the convection heat transfer and the obtained results provide a useful insight for enhancing heat transfer in two separate layers of nanofluid and porous medium inside complex-wavy cavity.*

Key words: *wavy enclosure, nanofluids, grid-transformations, multi-layers, Buongiorno's model*

Introduction

In the past few decades, the natural convection heat transfer in cavities has been received several attentions due to its industrial and environmental applications [1]. The heat transfer for the traditional fluids such as water, oil or ethylene glycol is enhanced by adding nanofluids. The nanofluid can enhance the heat transfer because it consist of nanoparticles with high thermal conductivity (*e. g.*, Al_2O_3, Cu or TiO_2). The term of the nanofluid was introduced by Choi in 1995 [2]. In the recent studies, several nanofluid models have been examined for estimating their heat transfer enhancement [3-12]. From the previous investigations [13-30], it is found that the nanofluids yield an effective enhancement in the heat transfer compared to base fluids with a low thermal conductivity (*e. g.*, water, oil, or ethylene glycol).

* Corresponding author, e-mails: ababdallah@kku.edu.sa; abdelreheam.abdallah@sci.svu.edu.eg

On the other hand, there are numerous studies related to the problem of the natural convection inside complex cavities due to its engineering applications. The applications include the manufactory of the cooling systems for microelectronic devices and underground cable systems. Adjlout *et al.* [31] studied the effect of a hot wavy wall on the natural convection in an inclined cavity. Misirlioglu *et al.* [32] investigated numerically, using the Galerkin finite element method (FEM), the free convection inside bent-wavy cavity saturated with a porous medium. Das and Mahmud [33] studied the thermal and hydrodynamic fluid behaviours inside wavy cavity. Raizah *et al.* [34] studied the natural convection flow in inclined open shallow cavities for a power-law non-Newtonian nanofluid. In addition, Aly *et al.* [35] investigated the effects of the wavy nanofluid/porous interface on the mixed convection of nanofluid-filled a double lid-driven cavity. Mahmud *et al.* [36] presented a numerical investigation of natural convection in an enclosure bounded by two isothermal wavy walls and two adiabatic straight walls. Oztop *et al.* [37] studied the convective heat transfer in wavy-walled enclosures under the effects of the volumetric heat sources. Ahmed *et al.* [38] studied numerically MHD mixed thermo-bio convection in porous cavity filled by oxytactic microorganism. Nagarajan *et al.* [39] investigated the effects of presence thin heater on MHD mixed convective flow and heat transfer for nanofluid-filled porous enclosure.

In the recent years, Aroon *et al.* [40] summarized the convective flow and heat transfer from wavy surfaces for viscous fluids, porous media, and nanofluids in heat transfer devices. Sheremet and Pop [41] studied the effects of sinusoidal temperature for side walls on natural convection in a wavy porous cavity filled with a nanofluid. In addition, Sheremet *et al.* [42] investigated the effects of thermal dispersion on free convection in a porous cavity filled with a nanofluid using Buongiorno's mathematical model. Sheremet *et al.* [43] modeled the free convection in an inclined wavy enclosure filled with a Cu-water nanofluid including isothermal heater at the corner. In addition, Sheremet *et al.* [44] studied the entropy generation in natural convection of nanofluid filled-wavy cavity. Hamid and Alireza [45] used the lattice Boltzmann method to investigate the hybrid nanofluid inside an open wavy cavity under the effects of a uniform magnetic field. Sheikholeslami *et al.* [46] applied FEM to report the effects of *V*-shaped fin angle on the CuO nanoparticles. In addition, Sheikholeslami [47] adopted a new recent method CVFEM to study the nanofluid MHD flow through complex shape of porous cavity. Sheikholeslami [22, 48-50], Sheikholeslami and Shehzad [51] introduced nice studies by applying innovative numerical method for the MHD nanofluid on complex cavities shapes under the effects of several physical circumstances and conditions. Javaherdeh *et al.* [52] introduced a numerical analysis for the natural convection in a wavy cavity filled with CuO-water nanofluid. In their model, one of the sinusoidal walls is maintained at the volatile high temperature and the opposite wavy wall is at a stable low temperature. For our knowledge, there are few studies related to the fluids with dispersed nanoparticles in a partitioned cavity [19, 53-55]. Moreover, there are no published studies related to the effect of the porous layers on the wavy cavity filled with the nanoparticles. Hence, the aim of this study is to investigate the enhancement heat transfer in nanofluid filled-wavy cavity saturated with a partially layered porous medium. The vertical walls of the cavity are taken as complex wavy geometries. The horizontal walls of the cavity are flat with insulated temperature. The complex wavy cavity is filled with a nanofluid and the upper half of the wavy cavity is saturated with the porous medium. The governing equations are formulated for the natural convection under the Boussinesq approximation in various regimes including pure-fluid, nanofluid, and porous medium. The effects of the geometric parameters of the wavy surface including amplitude ratio of the wavy surface, R,

and amplitude of the wavy surface, α_1, on the fluid-flows, heat transfer and nanoparticles volume fraction were investigated. The effects of the Rayleigh number, Darcy number, and nanofluid parameters on the overall heat transfer of nanofluid were also investigated. From the current investigation, the geometry parameters of the wavy surface have clear effects on the heat transfer improvement. Then, these parameters provide a useful insight for enhancing heat transfer in two separate layers of nanofluid and porous medium inside complex-wavy cavity. Overall, the results showed that the nanofluid parameters enhance the convection heat transfer and the obtained results provide a useful insight for enhancing heat transfer in nanofluid and porous medium layers inside the complex-wavy cavity.

Model description

Figure 1 presents the initial schematic diagram of a complex wavy cavity partially filled with the nanofluid and the porous medium. The left and right side walls are wavy walls, one of the sinusoidal walls is maintained at the high temperature, and the opposite wavy wall is at a low temperature. The bottom and the top walls of the cavity are adiabatic. The following points have been assumed in the current investigation:

– The height of the enclosure is mentioned by H, while the length of nanofluid layer is S.
– The inclination angle is denoted by γ, and the gravity acts in the normal direction.
– The left wavy wall of the enclosure is described by following dimensionless equations:

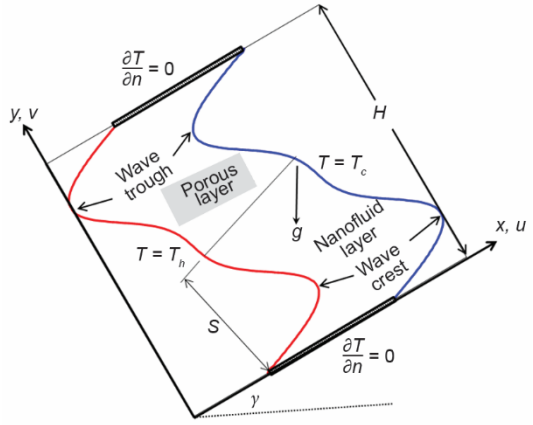

Figure 1. Initial schematic diagram for wavy cavity partially filled with nanofluid and porous medium

$$g_1(Y) = \alpha_1\left[\sin\left(\frac{2\pi Y}{\lambda}\right) + \mathrm{R}\sin\left(\frac{4\pi Y}{\lambda}\right)\right], \quad g_2(Y) = 1 + \alpha_1\left[\sin\left(\frac{2\pi Y}{\lambda}\right) + \mathrm{R}\sin\left(\frac{4\pi Y}{\lambda}\right)\right]$$

where α_1 is the amplitude of the sinusoidal function, λ – the wave length, and $\mathrm{R} = \alpha_1/\alpha_2$ – the is amplitude ratio.

– The flow is considered 2-D, unsteady and laminar and nanofluid is incompressible.
– The base fluid and nanofluids are in the thermal equilibrium and the flow is laminar.
– The two-phase model (Buongiorno's mathematical model) is applied to simulate case of nanofluid.
– The Brinkman's-extended Darcy model is applied to represent the flow inside the porous layer.
– The local thermal equilibrium model between porous medium and nanofluid is satisfied.
– All the fluid properties are assumed constants except the density which approximated by a linear Boussinesq approximation.
– The Joule heating, viscous dissipation and radiation effects are ignored.

Mathematical analysis

Taking into account all the previous assumptions, the continuity, momentum, energy, and nanoparticles volume fraction equations (in vorticity-stream function formula) are expressed as [19, 35, 56]:

$$\frac{\partial^2\psi}{\partial X^2}+\frac{\partial^2\psi}{\partial Y^2}=-\omega \tag{1}$$

$$\frac{\partial\omega}{\partial\tau}+\left[\chi\left(\frac{1}{\varepsilon}-1\right)+1\right]\left(\frac{\partial\psi}{\partial Y}\frac{\partial\omega}{\partial X}-\frac{\partial\psi}{\partial X}\frac{\partial\omega}{\partial Y}\right)=\mathrm{Pr}\left(\frac{\partial^2\omega}{\partial X^2}+\frac{\partial^2\omega}{\partial Y^2}\right)-\chi\frac{\varepsilon\,\mathrm{Pr}}{\mathrm{Da}}\omega+[\chi(\varepsilon-1)+1]\cdot$$
$$\cdot\mathrm{Pr}\,\mathrm{Ra}\left[\left(\frac{\partial\theta}{\partial X}-\mathrm{Nr}\frac{\partial\Phi}{\partial X}\right)\cos\gamma-\left(\frac{\partial\theta}{\partial Y}-\mathrm{Nr}\frac{\partial\Phi}{\partial Y}\right)\sin\gamma\right] \tag{2}$$

$$[\chi(\sigma-1)+1]\frac{\partial\theta}{\partial\tau}+\frac{\partial\psi}{\partial Y}\frac{\partial\theta}{\partial X}-\frac{\partial\psi}{\partial X}\frac{\partial\theta}{\partial Y}=[\chi(R_k-1)+1]\left(\frac{\partial^2\theta}{\partial X^2}+\frac{\partial^2\theta}{\partial Y^2}\right)+[\chi(\varepsilon-1)+1]\cdot$$
$$\cdot\left\{Nb\left(\frac{\partial\Phi}{\partial X}\frac{\partial\theta}{\partial X}+\frac{\partial\Phi}{\partial Y}\frac{\partial\theta}{\partial Y}\right)+Nt\left[\left(\frac{\partial\theta}{\partial X}\right)^2+\left(\frac{\partial\theta}{\partial Y}\right)^2\right]\right\} \tag{3}$$

$$\frac{\partial\Phi}{\partial\tau}+\left[\chi\left(\frac{1}{\varepsilon}-1\right)+1\right]\left(\frac{\partial\psi}{\partial Y}\frac{\partial\Phi}{\partial X}-\frac{\partial\psi}{\partial X}\frac{\partial\Phi}{\partial Y}\right)=\frac{1}{\mathrm{Le}}\left(\frac{\partial^2\Phi}{\partial X^2}+\frac{\partial^2\Phi}{\partial Y^2}\right)+\frac{Nt}{Nb\,\mathrm{Le}}\left(\frac{\partial^2\theta}{\partial X^2}+\frac{\partial^2\theta}{\partial Y^2}\right) \tag{4}$$

where

$$\chi=\begin{cases}0 & \text{in nanofluid layer } \varepsilon=1\\ 1 & \text{in porous layer } 0<\varepsilon<1\end{cases}$$

is a binary parameter to combine the dimensionless equations for the fluid layer and the porous layer in one system and:

$$\mathrm{Pr}=\frac{\nu}{\alpha_f},\quad \mathrm{Ra}=\frac{(1-\phi_0)\beta_{\mathrm{f}}g(T_{\mathrm{h}}-T_{\mathrm{c}})L^3}{\alpha_f\nu},\quad \mathrm{Da}=\frac{K}{L^2},\quad Nr=\frac{\phi_0(\rho_{\mathrm{p}}-\rho_{\mathrm{f}})}{(1-\phi_0)\beta_T\rho_{\mathrm{f}}(T_{\mathrm{h}}-T_{\mathrm{c}})}$$
$$Nb=\frac{D_B\phi_0(\rho C_p)_P}{\alpha_f(\rho C_p)_{\mathrm{f}}},\quad Nt=\frac{D_T\phi_0(\rho C_p)_p(T_{\mathrm{h}}-T_{\mathrm{c}})}{T_{\mathrm{c}}\alpha_f(\rho C_p)_{\mathrm{f}}},\quad \mathrm{Le}=\frac{\alpha_{\mathrm{f}}}{D_B},\quad R_k=\frac{k_m}{k_f},\quad \sigma=\frac{(\rho C_p)_m}{(\rho C_p)_f}$$

are Prandtl number, the Rayleigh number, the Darcy number, the buoyancy ratio, the dimensionless Brownian motion parameter, the dimensionless thermophoresis parameter, the Lewis number, the thermal conductivity ratio, and the ratio between the heat capacitances, respectively. In addition, the following dimensionless quantities are used to transform the governing equations to dimensionless form:

$$\tau=\frac{\alpha_f t}{L^2},\quad X=\frac{x}{L},\quad {}^\circ Y=\frac{y}{L},\quad {}^\circ U=\frac{uL}{\alpha_f},\quad {}^\circ V=\frac{vL}{\alpha_f},\quad {}^\circ P=\frac{(p+p_0)L^2}{\rho_r\alpha_f^2},\quad {}^\circ\theta=\frac{T-T_{\mathrm{c}}}{T_{\mathrm{h}}-T_{\mathrm{c}}},$$
$$\Phi=\frac{\phi}{\phi_0},\quad U=\frac{\partial\psi}{\partial Y},\quad V=-\frac{\partial\psi}{\partial X},\quad \omega=\frac{\partial V}{\partial X}-\frac{\partial U}{\partial Y} \tag{5}$$

The appropriate boundary conditions are:

– on the left wall $X = g_1(Y)$:

$$\psi = 0, \quad \omega = -\left(\frac{\partial^2\psi}{\partial X^2} + \frac{\partial^2\psi}{\partial Y^2}\right), \quad \theta = 1, \quad \phi = 1 \tag{6a}$$

– on the right wall $X = g_2(Y)$:

$$\psi = 0, \quad \omega = -\left(\frac{\partial^2\psi}{\partial X^2} + \frac{\partial^2\psi}{\partial Y^2}\right), \quad \theta = 0, \quad \phi = 0 \tag{6b}$$

– on the bottom wall $Y = 0$:

$$\psi = 0, \quad \omega = -\frac{\partial^2\psi}{\partial Y^2}, \quad \frac{\partial\theta}{\partial X^2} = 0, \quad \frac{\partial\phi}{\partial Y} = 0 \tag{6c}$$

– on the top wall $Y = A$:

$$\psi = 0, \quad \omega = -\frac{\partial^2\psi}{\partial Y^2}, \quad \frac{\partial\theta}{\partial Y} = 0, \quad \frac{\partial\phi}{\partial Y} = 0 \tag{6d}$$

The local Nusselt and Sherwood numbers at the wavy walls are defined:

$$\mathrm{Nu} = -[\chi(R_k - 1) + 1]\left\lfloor \frac{\partial\theta}{\partial X}\cos\varpi - \frac{\partial\theta}{\partial Y}\sin\varpi \right\rfloor \tag{7}$$

$$\mathrm{Sh} = -\left\lfloor \frac{\partial\phi}{\partial X}\cos\varpi - \frac{\partial\phi}{\partial Y}\sin\varpi \right\rfloor \tag{8}$$

The average Nusselt and Sherwood numbers are, also, expressed:

$$\mathrm{Nu}_{\mathrm{av}} = \frac{H}{H_w}\int_0^{H_w/H} \mathrm{Nu}\, \mathrm{d}S' \tag{9}$$

$$\mathrm{Sh}_{\mathrm{av}} = \frac{H}{H_w}\int_0^{H_w/H} \mathrm{Sh}\, \mathrm{d}S' \tag{10}$$

Numerical solution

The first step in solving the system of eqs. (1)-(4) is mapping the physical co-ordinates (X, Y) to the rectangular co-ordinates (ξ, η). To satisfy this objective, the new independent variables ξ and η are introduced:

$$\xi = X - \alpha_1\left[\sin\left(\frac{2\pi Y}{\lambda}\right) + \mathrm{R}\sin\left(\frac{4\pi Y}{\lambda}\right)\right], \quad \eta = Y \tag{11}$$

Substituting eq. (11) into the governing eqs. (1)-(4), the following system is obtained:

$$\left[\left(\frac{\partial\xi}{\partial X}\right)^2 + \left(\frac{\partial\xi}{\partial Y}\right)^2\right]\frac{\partial^2\psi}{\partial\xi^2} + 2\frac{\partial\xi}{\partial Y}\frac{\partial^2\psi}{\partial\eta\partial\xi} + \frac{\partial^2\psi}{\partial\eta^2} + \frac{\partial^2\xi}{\partial Y^2}\frac{\partial\psi}{\partial\xi} = -\omega \tag{12}$$

$$\frac{\partial\omega}{\partial\tau}+\left[\chi\left(\frac{1}{\varepsilon}-1\right)+1\right]\left(\frac{\partial\psi}{\partial\eta}\frac{\partial\omega}{\partial\xi}\frac{\partial\xi}{\partial X}-\frac{\partial\psi}{\partial\xi}\frac{\partial\xi}{\partial X}\frac{\partial\omega}{\partial\eta}\right)=$$

$$=\mathrm{Pr}\left\{\left[\left(\frac{\partial\xi}{\partial X}\right)^2+\left(\frac{\partial\xi}{\partial Y}\right)^2\right]\frac{\partial^2\omega}{\partial\xi^2}+2\frac{\partial\xi}{\partial Y}\frac{\partial^2\omega}{\partial\eta\partial\xi}+\frac{\partial^2\omega}{\partial\eta^2}+\frac{\partial^2\xi}{\partial Y^2}\frac{\partial\omega}{\partial\xi}\right\}-$$

$$-\chi\frac{\varepsilon\,\mathrm{Pr}}{\mathrm{Da}}\omega+\varepsilon[\chi(\varepsilon-1)+1]\,\mathrm{Pr}\,\mathrm{Ra}\left\{\left[\left(\frac{\partial\xi}{\partial X}\frac{\partial\Theta}{\partial\xi}-Nr\frac{\partial\xi}{\partial X}\frac{\partial\Phi}{\partial\xi}\right)\cos\gamma\right]-\right.$$

$$\left.-\left[\frac{\partial\Theta}{\partial\xi}\frac{\partial\xi}{\partial Y}+\frac{\partial\Theta}{\partial\eta}-Nr\left(\frac{\partial\Phi}{\partial\xi}\frac{\partial\xi}{\partial Y}+\frac{\partial\Phi}{\partial\eta}\right)\right]\sin\gamma\right\} \tag{13}$$

$$[\chi(\sigma-1)+1]\frac{\partial\theta}{\partial\tau}+\frac{\partial\psi}{\partial\eta}\frac{\partial\xi}{\partial X}\frac{\partial\theta}{\partial\xi}-\frac{\partial\psi}{\partial\xi}\frac{\partial\xi}{\partial X}\frac{\partial\theta}{\partial\eta}=[\chi(R_k-1)+1]\cdot$$

$$\cdot\left\{\left[\left(\frac{\partial\xi}{\partial X}\right)^2+\left(\frac{\partial\xi}{\partial Y}\right)^2\right]\frac{\partial^2\theta}{\partial\xi^2}+2\frac{\partial\xi}{\partial Y}\frac{\partial^2\theta}{\partial\eta\partial\xi}+\frac{\partial^2\theta}{\partial\eta^2}+\frac{\partial^2\xi}{\partial Y^2}\frac{\partial\theta}{\partial\xi}\right\}+[\chi(\varepsilon-1)+1]\cdot$$

$$\cdot\left\{Nb\left[\left(\frac{\partial\xi}{\partial X}\right)^2+\left(\frac{\partial\xi}{\partial Y}\right)^2\frac{\partial\Phi}{\partial\xi}\frac{\partial\theta}{\partial\xi}+\frac{\partial\xi}{\partial Y}\left(\frac{\partial\Phi}{\partial\xi}\frac{\partial\theta}{\partial\eta}+\frac{\partial\Phi}{\partial\eta}\frac{\partial\theta}{\partial\xi}\right)+\frac{\partial\Phi}{\partial\eta}\frac{\partial\theta}{\partial\eta}\right]+\right.$$

$$\left.+Nt\left[\left(\frac{\partial\xi}{\partial X}\right)^2+\left(\frac{\partial\xi}{\partial Y}\right)^2\right]\left(\frac{\partial\theta}{\partial\xi}\right)^2+2\frac{\partial\xi}{\partial Y}\frac{\partial\theta}{\partial\xi}\frac{\partial\theta}{\partial\eta}+\left(\frac{\partial\theta}{\partial\eta}\right)^2\right\} \tag{14}$$

$$\frac{\partial\Phi}{\partial\tau}+\left[\chi\left(\frac{1}{\varepsilon}-1\right)+1\right]\left(\frac{\partial\psi}{\partial\eta}\frac{\partial\xi}{\partial X}\frac{\partial\Phi}{\partial\xi}-\frac{\partial\psi}{\partial\xi}\frac{\partial\xi}{\partial X}\frac{\partial\Phi}{\partial\eta}\right)=$$

$$=\frac{1}{\mathrm{Le}}\left\{\left[\left(\frac{\partial\xi}{\partial X}\right)^2+\left(\frac{\partial\xi}{\partial Y}\right)^2\right]\frac{\partial^2\Phi}{\partial\xi^2}+2\frac{\partial\xi}{\partial Y}\frac{\partial^2\Phi}{\partial\eta\partial\xi}+\frac{\partial^2\Phi}{\partial\eta^2}+\frac{\partial^2\xi}{\partial Y^2}\frac{\partial\Phi}{\partial\xi}\right\}+$$

$$+\frac{Nt}{Nb\,\mathrm{Le}}\left\{\left[\left(\frac{\partial\xi}{\partial X}\right)^2+\left(\frac{\partial\xi}{\partial Y}\right)^2\right]\frac{\partial^2\theta}{\partial\xi^2}+2\frac{\partial\xi}{\partial Y}\frac{\partial^2\theta}{\partial\eta\partial\xi}+\frac{\partial^2\theta}{\partial\eta^2}+\frac{\partial^2\xi}{\partial Y^2}\frac{\partial\theta}{\partial\xi}\right\} \tag{15}$$

The dimensionless boundary conditions are converted to:

$$\xi=0,\quad 0\le\eta\le A:\psi=0,\quad \omega=-\frac{\delta}{J^2}\frac{\partial^2\psi}{\partial\xi^2}\theta=1,\quad \Phi=1 \tag{16}$$

$$\xi=1,\quad 0\le\eta\le A:\psi=0,\quad \omega=-\frac{\delta}{J^2}\frac{\partial^2\psi}{\partial\xi^2}\theta=0,\quad \Phi=0 \tag{17}$$

$$\eta=1,\quad 0\le\xi\le1:\psi=0,\quad \omega=-\frac{\vartheta}{J^2}\frac{\partial^2\psi}{\partial\eta^2},\quad \frac{\partial\theta}{\partial\eta}=0,\quad \frac{\partial\Phi}{\partial\eta}=0 \tag{18}$$

The local Nusselt and Sherwood numbers at the side walls are defined:

$$\mathrm{Nu} = -[\chi(R_k - 1) + 1]\left[\frac{\partial\theta}{\partial\xi}(\xi_X \cos\varpi - \xi_Y \sin\varpi) + \frac{\partial\theta}{\partial\eta}(\eta_X \cos\varpi - \eta_Y \sin\varpi)\right] \tag{19}$$

$$\mathrm{Nu} = -\left[\frac{\partial\Phi}{\partial\xi}(\xi_X \cos\varpi - \xi_Y \sin\varpi) + \frac{\partial\Phi}{\partial\eta}(\eta_X \cos\varpi - \eta_Y \sin\varpi)\right] \tag{20}$$

Secondly, the fully implicit finite volume method is applied to solve the resulting system (12)-(15) subjected to the boundary conditions (16). The central differences scheme is used to approximate the first and second derivatives. However, the time derivatives are approximated using the backward scheme. The alternate difference implicit scheme is applied to solve the resulting algebraic system. In-house code written in FORTRAN 90 (programming language) for implicit finite volume method was used during this study. The grid size (121×121) is selected after producing a grid-independent study, tab. 1, while the time step $\Delta\tau = 10^{-4}$ is used for all computations. For convergence to the steady state it is assumed that for any dependent variable φ:

Table 1. Grid study at *Nr* = *Nt* = 0.1, Ra = 10^4, Da = 10^{-3}, λ = 2, α_1 = 0.50, R = 1/2.5, Pr = 6.28, Le = 10, γ = 30°, ε = 0.6

Grids	$\psi_{\min}$
31×31	–5.6919270
41×41	–5.4126310
61×61	–5.1517150
81×81	–5.0272490
101×101	–4.9535170
121×121	–4.9042870

$$\left|\frac{\varphi_{i,j}^{k} - \varphi_{i,j}^{k-1}}{\varphi_{i,j}^{k-1}}\right| \le 10^{-6} \tag{21}$$

In order to check the accuracy of the present results, comparisons with previously published results are performed and presented in fig. 2. It is observed that there are very good agreements between the present results and those obtained by Cho and Chen [57]. In addition, in order to choose the suitable grid for these calculations, a numerical test by using several grids started from [31×31] to [121×121] have been introduced in tab. 1. In this table, we showed that the grid independence study of minimum stream function at *Nr* = *Nt* = 0.1, Ra = 10^4, Da = 10^{-3}, λ = 2, α_1 = 0.50, R = 1/2.5, Pr = 6.28, Le = 10, γ = 30°, ε = 0.6. It is noted that a [121×121] uniform grid is found to meet the requirements of both the grid independence study and the computational time limits.

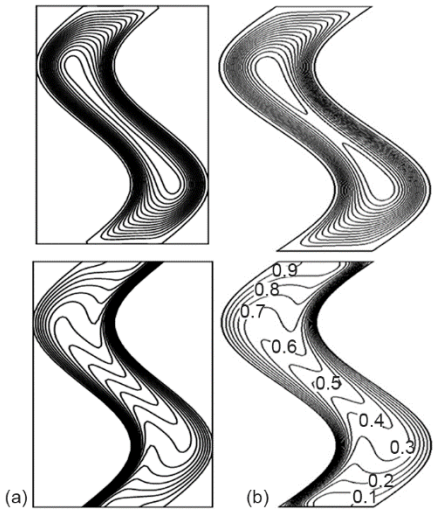

Figure 2. Comparison of the present results (a) and those obtained by Cho and Chen [57] (b)

Results and discussion

In this section, the simulations of the natural convection for a nanofluid filled-complex wavy cavity saturated with a partially layered porous medium. The non-dimensional parameters were assigned: Rayleigh number ($10^3 \le \mathrm{Ra} \le 10^5$), Darcy parameter ($10^{-6} \le \mathrm{Da} \le 10^{-3}$), thermophoresis parameter ($0.1 \le Nt \le 0.5$), nanofluid buoyancy ratio

($0.1 \le Nr \le 0.5$), Brownian motion parameter ($0.1 \le Nb \le 0.5$), inclination angle ($0° \le \gamma \le 90°$). Geometry parameters: Amplitude ratio of the wavy surface, R, and amplitude of the wavy surface, α_1, were taken as $\alpha_1 = 0.50$, R = 1/2.5, $\alpha_1 = 0.470$, R = 2.5/1, and $\alpha_1 = 0.670$, R = 0.0. During the whole simulations, the base fluid is taken as pure water with Pr = 6.28 and the porosity is applied as $\varepsilon = 0.6$. The obtained results from the current investigation are presented in graphical forms by the streamlines, dimensionless temperatures (isotherms), nanoparticles volume fraction, local Nusselt number, and the local Sherwood number.

Effects of Rayleigh number

Figure 3 shows the effect of Rayleigh number on the streamlines, isotherms, and nanoparticles volume fraction. Generally, at higher Rayleigh numbers (stronger buoyancy force), the natural convection inside the wavy cavity becomes stronger and the convective transport is enhanced. In the current investigation, fig. 3 shows the increase on the streamlines intensity according to an increase on the Rayleigh number from Ra = 10^3 to Ra = 10^5. Also, as the Rayleigh

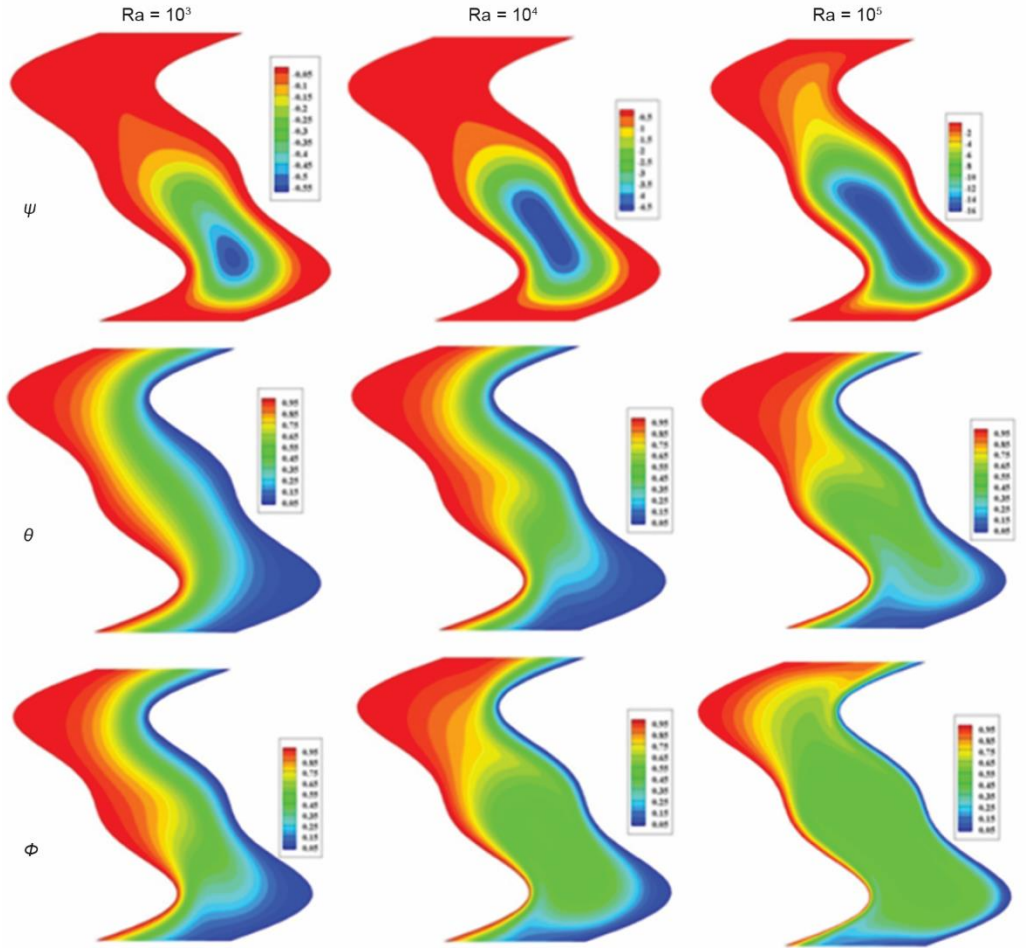

Figure 3. Effect of Rayleigh number on the streamlines, isotherms, and nanoparticles volume fraction when *Nb* = *Nr* = *Nt* = 0.1, Da = 10^{-3}, λ = 2, α_1 = 0.50, R = **1/2.5, Pr = 6.28, Le = 10, γ = 30°, ε = 0.6**
(*for color image see journal web site*)

number increases then the streamlines are highly penetrate through the porous structures, which are located on the top part of the wavy cavity. The isotherms are transformed from the vertical distributions (conduction regime) to the stratified patterns (convection regime) with increasing Rayleigh number. Also, the nanoparticles volume fractions are changed from the purely vertical lines along the wavy cavity to the stratified patterns. As a result, the local Nusselt and local Sherwood numbers along the hot wavy-wall also depend on the values of the Rayleigh number, as shown in fig. 4. Both of the local Nusselt and local Sherwood numbers increase according to the increase on the Rayleigh number especially at the lower region of the hot wavy cavity due to larger gradients of the temperature and nanoparticles volume fraction at this region.

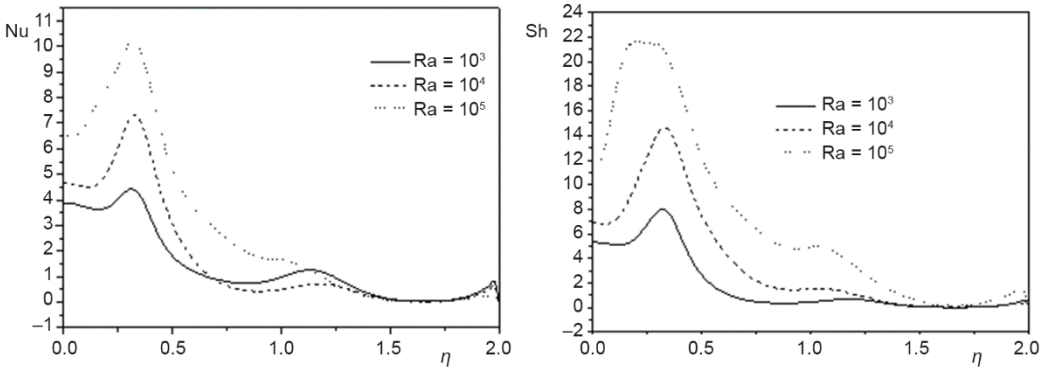

Figure 4. Profiles of local Nusselt and local Sherwood numbers for different values of Rayleigh number when *Nb* = *Nr* = *Nt* = 0.1, Da = 10^{-3}, λ = 2, α_1 = 0.50, R **= 1/2.5, Pr = 6.28, Le = 10, γ = 30°, ε = 0.6**

Effects of Darcy number

Figure 5 shows the effects of Darcy number on the streamlines, temperature, and nanoparticles volume fraction. Distributions of the streamlines show that increasing Darcy number from 10^{-6} to 10^{-3} increase the penetration of the nanofluid through the porous layer due to the increased permeability. The isotherms transit from the conduction regime to the convection regime at high Darcy number Da = 10^{-3}. The nanoparticles volume fraction lines are highly penetrate through the porous layer with horizontal distributions at high Darcy number Da = 10^{-3}. It is noted that, the porous medium layer acts as a rigid body against the fluid-flow. There are almost no changes on the local Nusselt and local Sherwood numbers along the hot wavy-wall under the effects of the Darcy number. On the crest region of the top wavy cavity, the local Nusselt and local Sherwood numbers are decrease as the Darcy number decreases from 10^{-3} to 10^{-6}, fig. 6.

Effects of nanofluid parameters

Figures 7-9 show the effects of the thermophoresis parameter, *Nt*, nanofluid buoyancy ratio, *Nr,* and Brownian motion parameter, *Nb,* on the streamlines, isotherms, and nanoparticles volume fraction, respectively. As the *Nt* increases from 0.1 to 0.5, then the streamlines and isotherms have a slight enhancement in their strengths. While, the nanoparticles volume fraction lines were affected clearly by increasing the thermophoresis parameter. The patterns of the nanoparticles volume fraction are change to almost parallel distributions along the horizon tal lines. As the *Nr* increases from 0.1 to 0.5, then the penetration of the streamlines across the porous layer decreases. The isothermal lines have a slight change according to variations on the

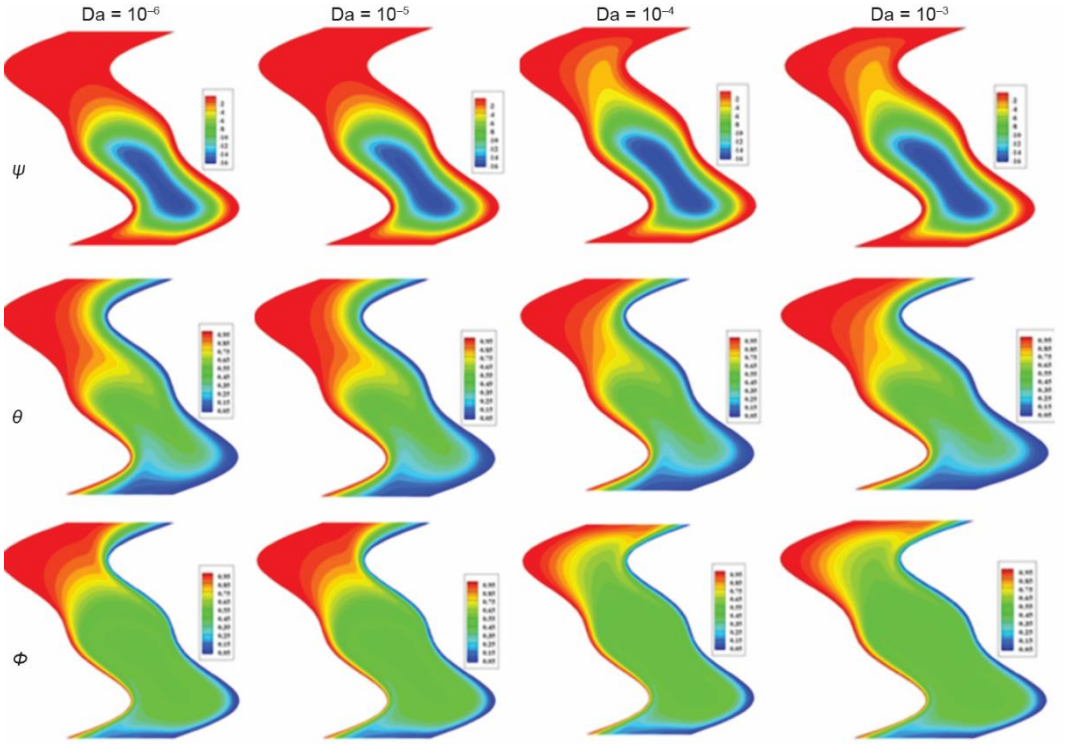

Figure 5. Effect of Darcy number on streamlines, isotherms, and nanoparticles volume fraction when *Nb* = *Nr* = *Nt* = 0.1, Ra = 10^5, λ = 2, α_1 = 0.50, R = 1/2.5, Pr = 6.28, Le = 10, γ = 30°, ε = 0.6
(*for color image see journal web site*)

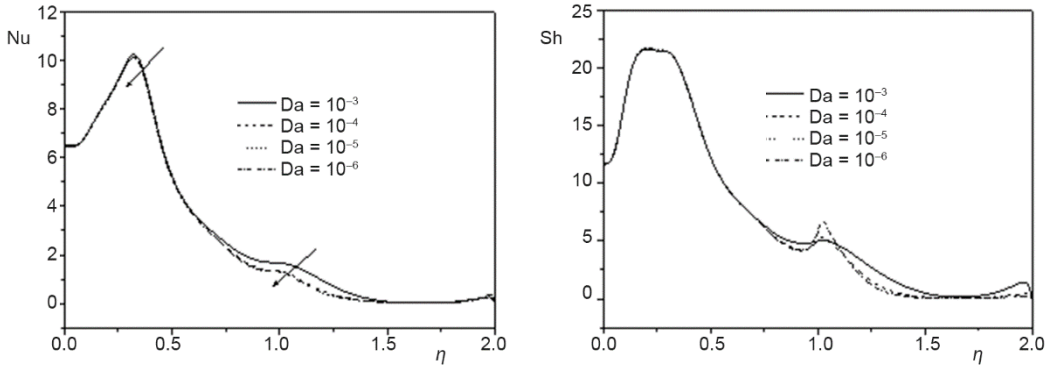

Figure 6. Profiles of the local Nusselt number and the local Sherwood number for different values of Darcy number when *Nb* = *Nr* = *Nt* = 0.1, Ra = 10^5, λ = 2, α_1 = 0.50, R = 1/2.5, Pr = 6.28, Le = 10, γ = 30°, ε = 0.6

Nr. The nanoparticles volume fraction change their patterns at the center of the wavy cavity from the wide circulation to small circulation. The *Nb* has also a slight effect on the streamlines and isotherms. The variation on the *Nr* varies the distributions of the nanoparticles volume fractions patters across the wavy cavity.

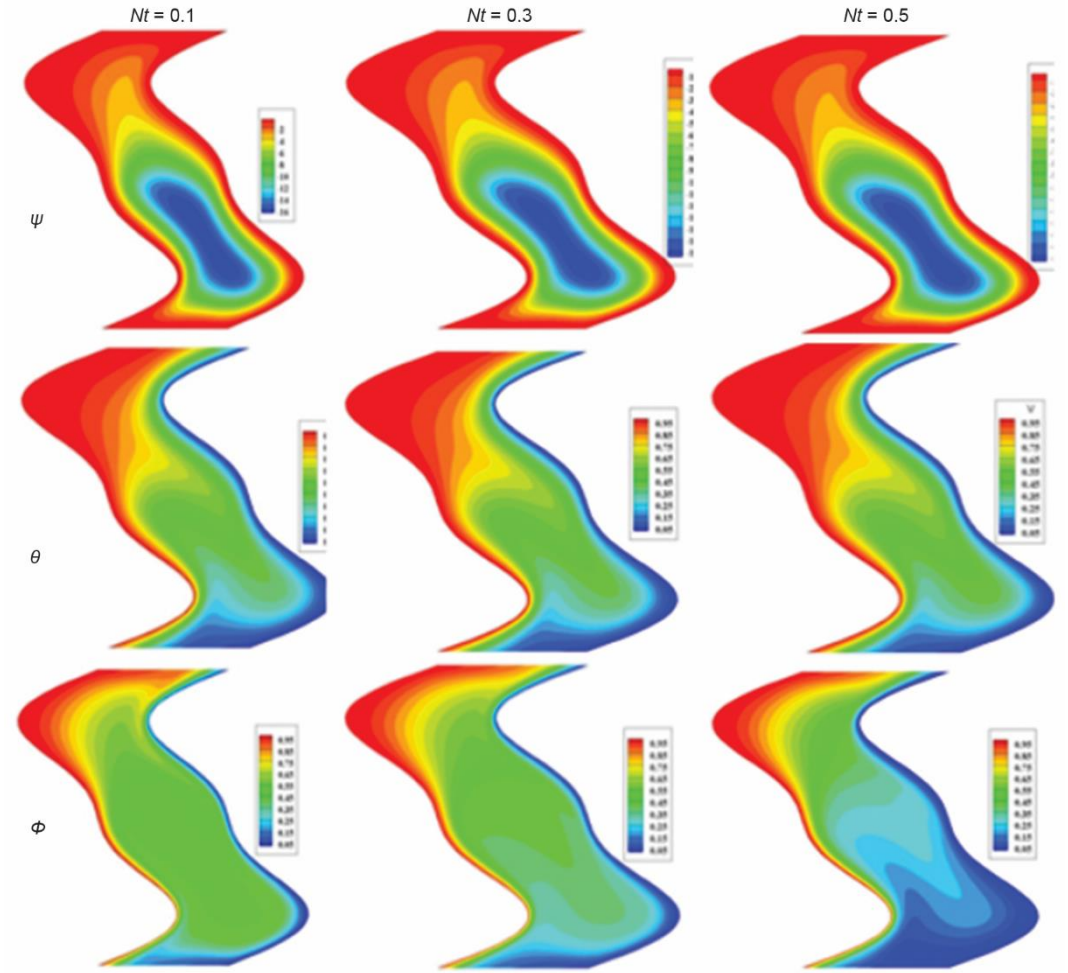

Figure 7. Effect of *Nt* on the streamlines, isotherms, and nanoparticles volume fraction when *Nb* = *Nr* = 0.1, Ra = 10^5, Da = 10^{-3}, λ = 2, α_1 = 0.50, R **= 1/2.5, Pr = 6.28, Le = 10, γ = 30°, ε = 0.6**
(*for color image see journal web site*)

In addition, the variations of the local Nusselt and local Sherwood numbers along the hot wavy-wall under the effects of the *Nt*, *Nr,* and *Nb* have been introduced in figs. 10-12. The profiles of the local Nusselt number are decrease according to an increase on the *Nt*, *Nr*, and *Nb*. The local Sherwood number increases as the *Nt* and *Nb* increase, while it decreases as the *Nr* increases.

Effects of geometry parameters

Figures 13 and 14 show the effects of the inclination angle, γ, and amplitude ratio of the wavy surface (α_1 and R) on the streamlines, isotherms, and nanoparticles volume fraction, respectively. The obtained results from fig. 13 show that when γ = 0°, the streamlines distributions are denser on the nanofluid layer compare to the porous medium layer. As the inclination angle increases to γ = 30°, the intensity of streamlines increases with more denser on the nanofluid layer and penetrations through the porous layer were occurred. Extremely increasing

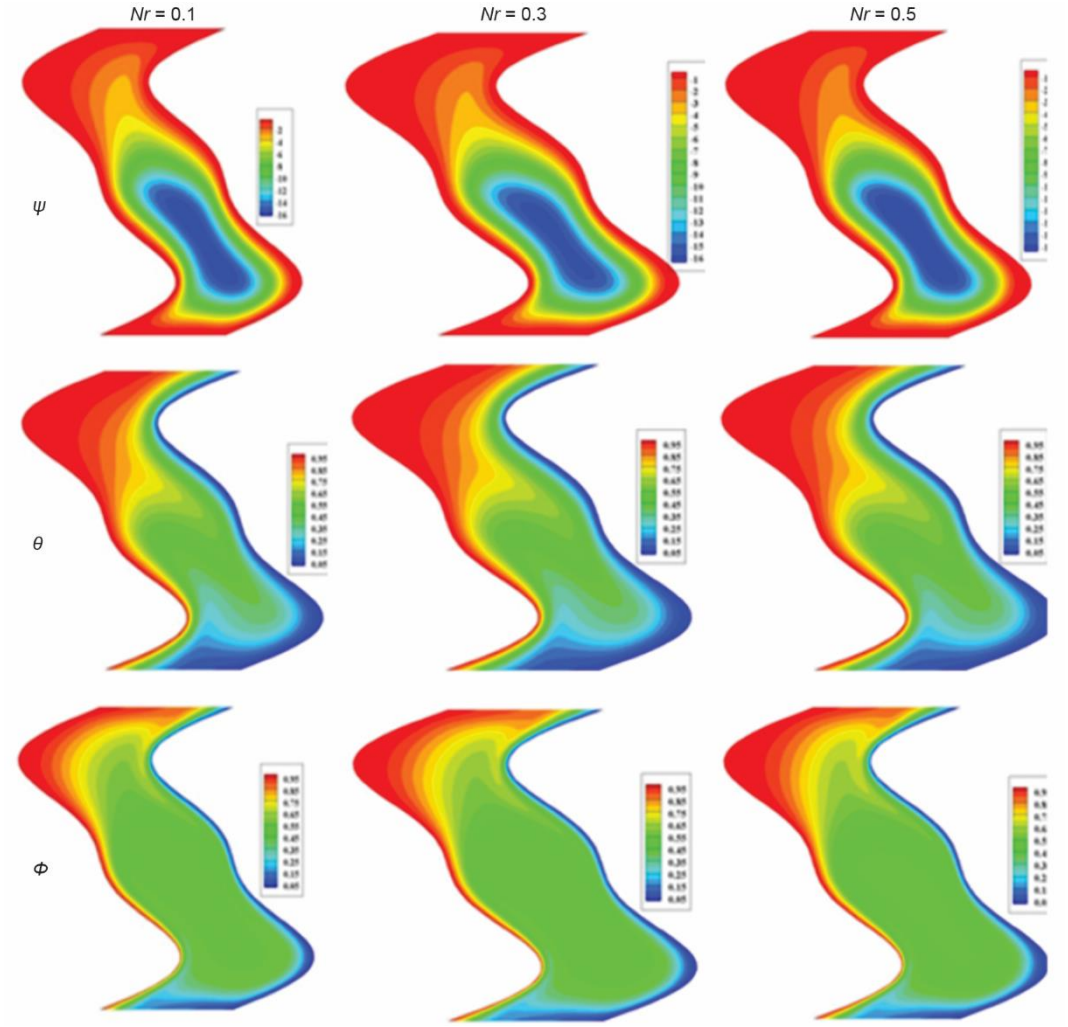

Figure 8. Effect of *Nr* on the streamlines, isotherms , and nanoparticles volume fraction when *Nb* = *Nt* = 0.1, Ra = 10^5, Da = 10^{-3}, λ = 2, α_1 = 0.50, R = **1/2.5, Pr = 6.28, Le = 10, γ = 30°, ε = 0.6** (*for color image see journal web site*)

of the inclination angle to $\gamma = 60°$ and $\gamma = 90°$, the streamlines generate two separate circulations at $\gamma = 60°$ and three separate circulations at $\gamma = 90°$. The denser circulations with intensified flows were generated on the nanofluid layer, which strengthen the convection. The isotherms change their distributions and manifest the convection in both of the nanofluid and porous layers according to an increase on the an inclinations angle γ from 0° and 90°. Also, an inclinations angle γ from 0° and 90°, then the nanoparticles volume fraction patterns change their distributions from the mostly vertical lines across the wavy surface within one circulation at the centre to the several circulations and denser lines across the wavy surface.

Figure 14 depicts the effects of α_1 and R on the streamlines, isotherms, and nanoparticles volume fraction. From this figure, the patterns of the streamlines, isotherms, and nanoparticles volume fraction are strongly dependent on the amplitude ratio (*i. e.*, waveform) of the

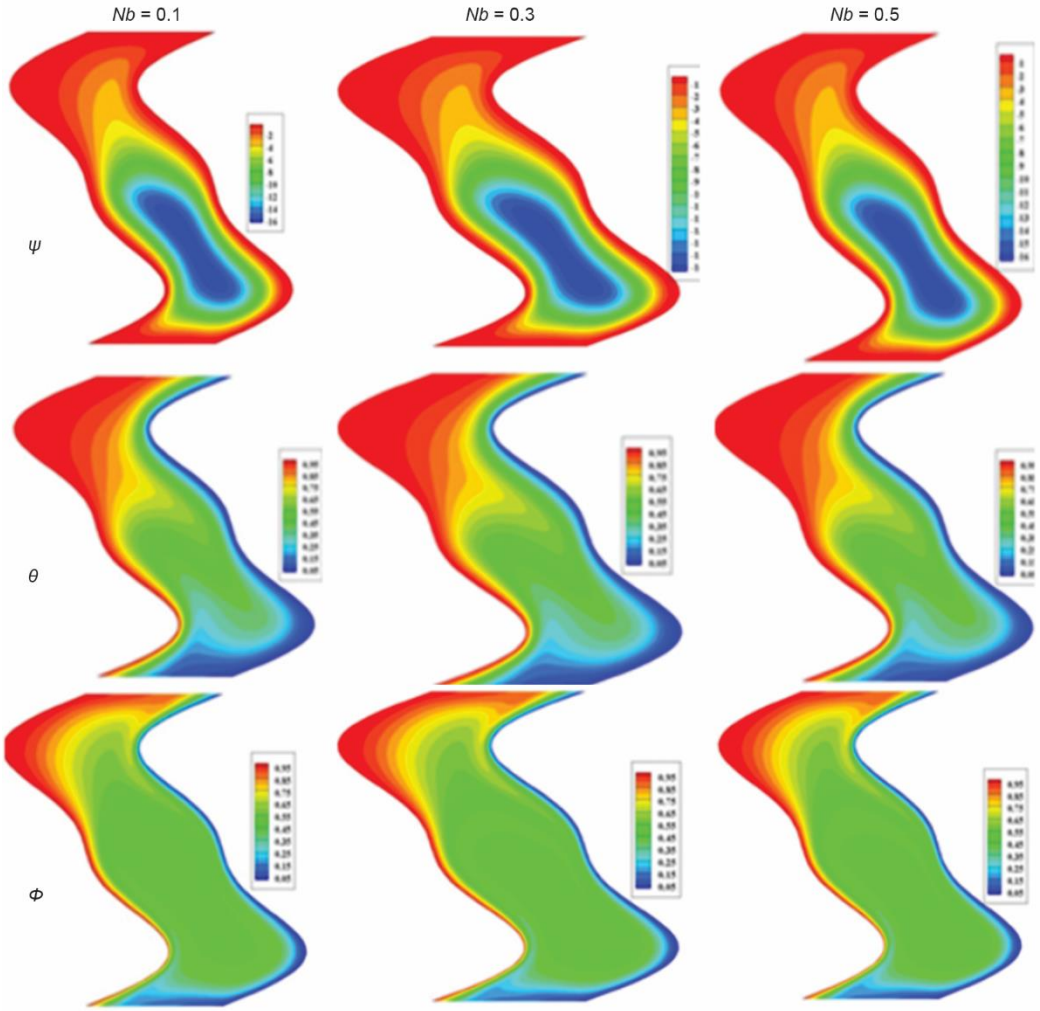

Figure 9. Effect of *Nb* on the streamlines, isotherms, and nanoparticles volume fraction when *Nr* = *Nt* = 0.1, Ra = 10^5, Da = 10^{-3}, λ = 2, α_1 = 0.50, R **= 1/2.5, Pr = 6.28, Le = 10, γ = 30°, ε = 0.6** (*for color image see journal web site*)

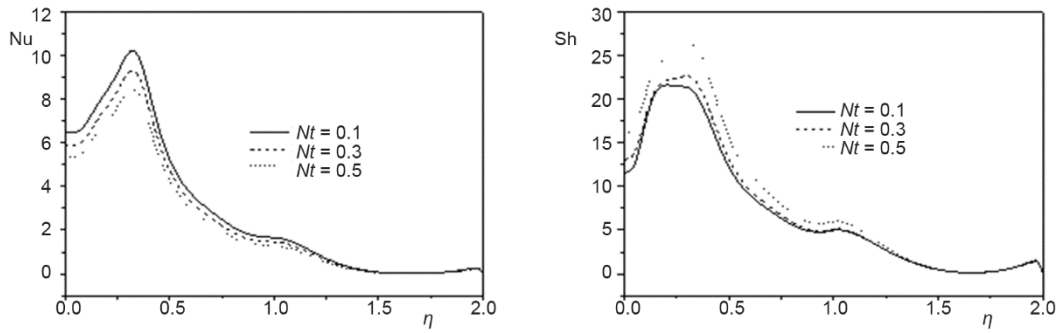

Figure 10. Profiles of the local Nusselt and local Sherwood numbers for different values of *Nt* when *Nb* = *Nr* = 0.1, Ra = 10^5, Da = 10^{-3}, λ = 2, α_1 = 0.50, R **= 1/2.5, Pr = 6.28, Le = 10, γ = 30°, ε = 0.6**

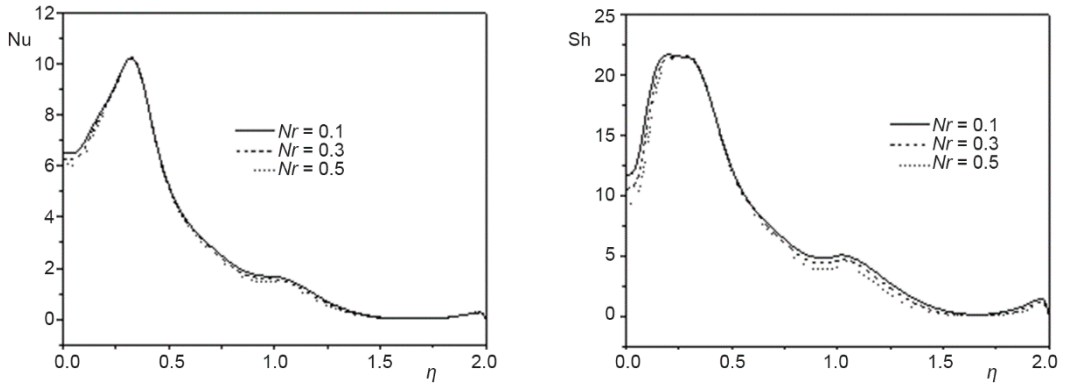

Figure 11. Profiles of the local Nusselt and local Sherwood numbers for different values of *Nr* when *Nb* = *Nt* = 0.1, Ra = 10^5, Da = 10^{-3}, λ = 2, α_1 = 0.50, R = **1/2.5, Pr = 6.28, Le = 10, γ = 30°, ε = 0.6**

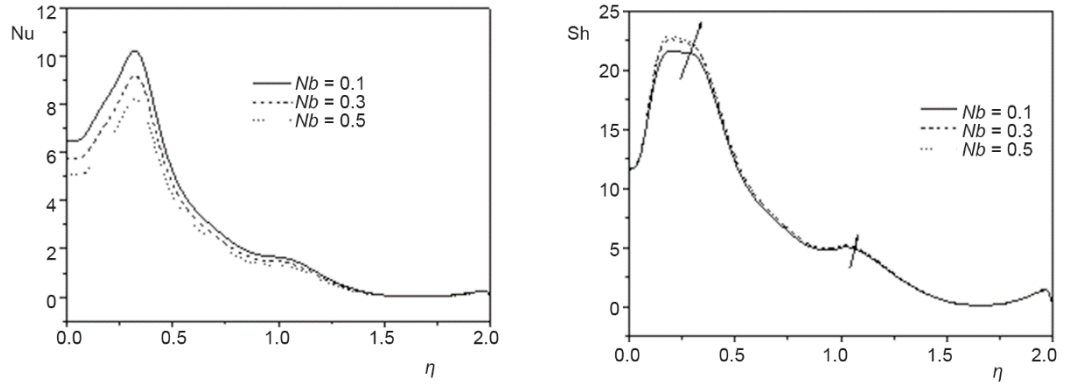

Figure 12. Profiles of local Nusselt and local Sherwood numbers for different *Nb* when *Nt* = *Nr* = 0.1, Ra = 10^5, Da = 10^{-3}, λ = 2, α_1 = 0.50, R = **1/2.5, Pr = 6.28, Le = 10, γ = 30°, ε = 0.6**

complex-wavy surface. At α_1 = 0.50, R = 1/2.5, the streamlines are denser on the nanofluid layer and are still penetrate through the porous layer. When α_1 = 0.470, R = 2.5/1, the streamlines generate three main separate circulations along the wavy surface. The denser circulation occur on the nanofluid layer and the lighter one occur on the porous layer. While at α_1 = 0.670, R = 0.0, only two circulations of the streamlines are formed on the wavy surface with denser one on the nanofluid layer and lighter on the porous layer. In addition, it is seen that, the different waveforms induce different flow patterns of the isotherms and nanoparticles volume fraction distributions. Figure 15 illustrates the profiles of the local Nusselt and local Sherwood numbers under the effects of different values of γ. The local Nusselt number decreases as the inclination angle increases γ from 0° to 90° at the lower region of the wavy cavity, while it increases at the crest region of the wavy cavity. In addition, the local Sherwood number has similar tendencies as it decreases as the inclination angle increases γ at the lower region of the wavy cavity and it increases at the crest region of the wavy cavity.

Conclusion

A computational study has been performed on the natural convection in a nanofluid-filled inclined wavy cavity saturated with a partially layered porous medium. The complex

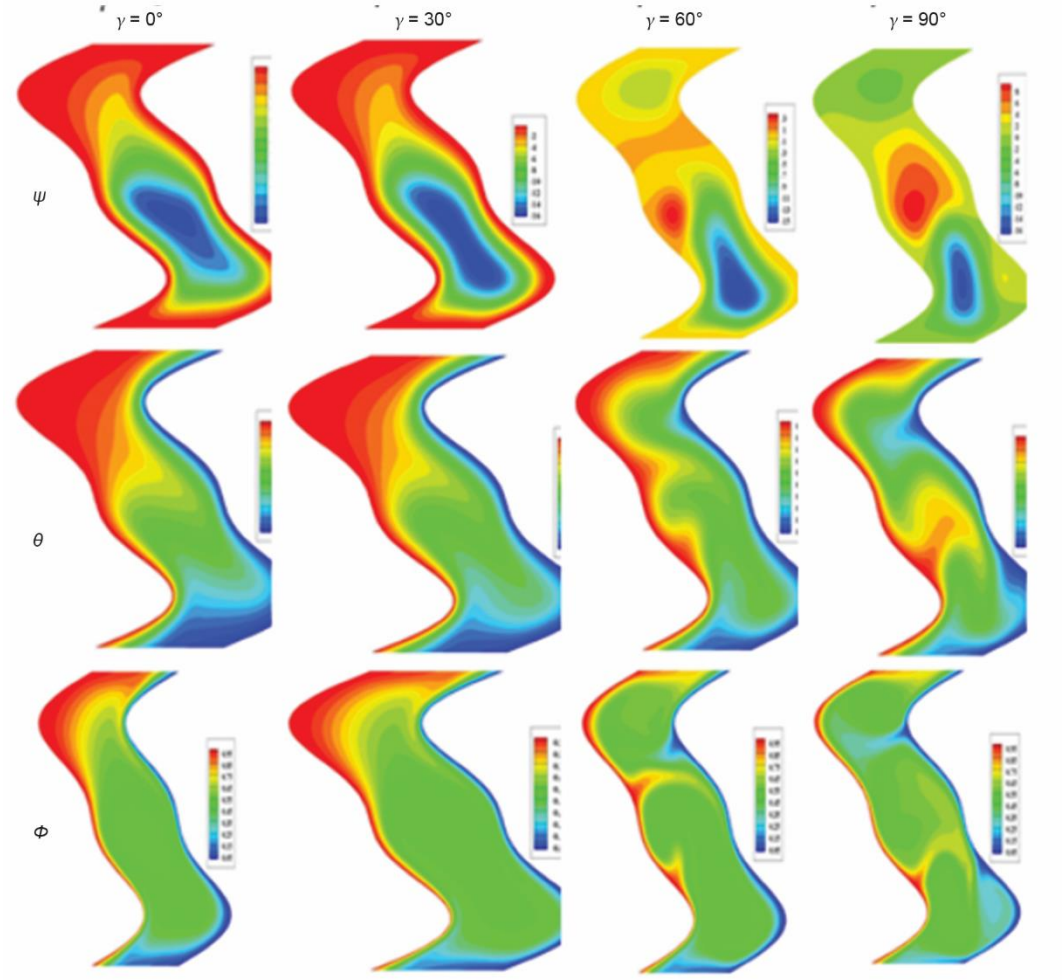

Figure 13. Effects of the inclination angle γ on the streamlines, isotherms, and nanoparticles volume fraction when $Nr = Nt = Nb = 0.1$, $Ra = 10^5$, $Da = 10^{-3}$, $\lambda = 2$, $\alpha_1 = 0.50$, R = 1/2.5, Pr = 6.28, Le = 10, $\gamma = 30°$, $\varepsilon = 0.6$ (*for color image see journal web site*)

wavy cavity is filled with a nanofluid and the upper half of the wavy cavity is saturated with porous medium.

The obtained results have led to the following concluding points:

- At higher Rayleigh number (stronger buoyancy force), the convection inside the wavy cavity becomes stronger with more penetrations of nanofluid through the porous layer.
- At higher Darcy number (higher permeability of the porous media), the nanofluid penetrate more through the porous layer.
- The local Nusselt number decreases as the *Nt, Nr,* and *Nb* increase.
- The local Sherwood number increases, as both of the *Nt* and *Nb* increase, while it decreases as the *Nr* increases.
- The stream, isothermal, and nanoparticles volume fraction lines are strongly affected by the geometry parameters of the wavy cavity.

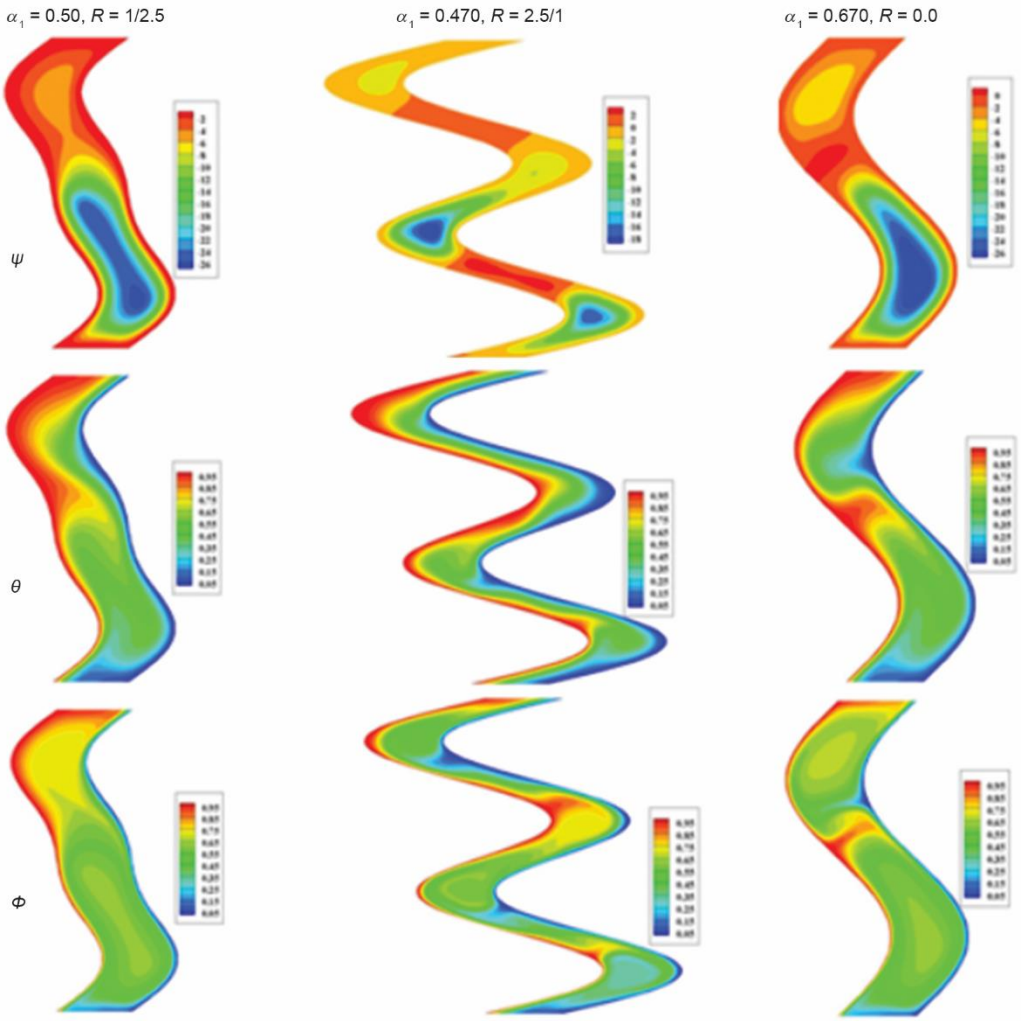

Figure 14. Effects of α_1 and R on the streamlines, isotherms, and nanoparticles volume fraction when $Nr = Nt = Nb = 0.1$, $Ra = 10^5$, $Da = 10^{-3}$, $\lambda = 4$, $\gamma = 30°$, $Pr = 6.28$, $Le = 10$, $\gamma = 30°$, $\varepsilon = 0.6$
(*for color image see journal web site*)

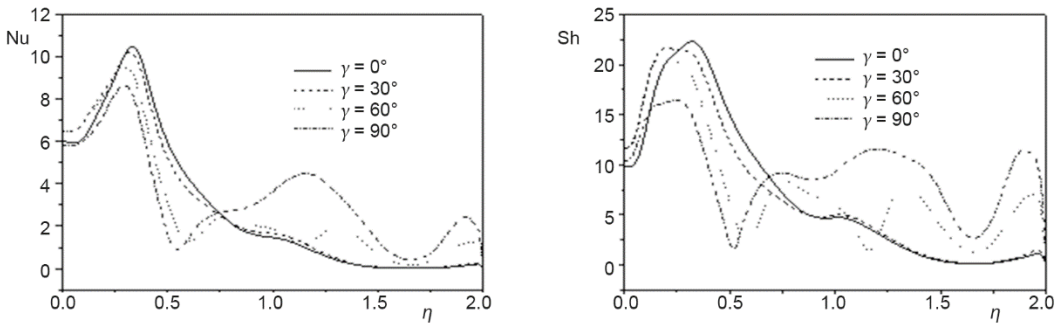

Figure 15. Profiles of the local Nusselt and local Sherwood numbers for different values of γ when $Nb = Nr = Nt = 0.1$, $Ra = 10^5$, $Da = 10^{-3}$, $\lambda = 2$, $\alpha_1 = 0.50$, R = 1/2.5, $Pr = 6.28$, $Le = 10$, $\gamma = 30°$, $\varepsilon = 0.6$

Acknowledgment

The authors extend their appreciation to the Deanship of Scientific Research at Jouf University for funding this work though General Project under grant number (810/39).

Nomenclature

C_p – specific heat
Da – Darcy parameter
D_B – Brownian diffusion coefficient, [m^2s^{-1}]
D_T – thermophoresis diffusion coefficient, [m^2s^{-1}]
H – enclosure height
H_w – arc-length of the side wall
K – permeability, [m^2]
L – length scale
Le – Lewis number
Nb – Brownian motion parameter
Nr – buoyancy ratio
Nt – thermophoresis parameter
Nu – Nusselt number
P – Pressure, [Nm^{-2}]
Pr – Prandtl number
Ra – Rayleigh number
R – amplitude ratio
S – length of nanofluid layer
S' – tangent of the side wall
Sh – Sherwood number
T – temperature, [K]
u, v – dimension velocity components, [ms^{-1}]
U, V – dimensionless velocity components
X, Y – dimensionless co-ordinates
x, y – cartesian co-ordinates, [m]

Greek symbols

α_1 – amplitude of the sinusoidal function
α_f – thermal diffusivity, [m^2s^{-1}]
β – thermal expansion coefficient, [K^{-1}]
γ – inclination angle, [°]
ε – porosity
λ – wave length
μ – viscosity
ν – kinematic viscosity, [m^2s^{-1}]
ϖ – any point inclination on side walls from Y-axis
ρ – density, [kgm^3]
σ – capacity ratio
τ – dimensionless time
Φ – solid volume fraction
χ – layer recognition
ψ – stream function, [m^2s^{-1}]
ω – vorticity

Subscripts

c – cold
h – hot
f – fluid
p – dispersed nanoparticles

References

[1] Ostrach, S., Natural Convection in Enclosures. *Journal of Heat Transfer*, *110* (1988), 4b, pp. 1175-1190
[2] Chol, S., Enhancing Thermal Conductivity of Fluids with Nanoparticles*, Proceedings,* International Mechanical Engineering Congress and Exhibition, San Francisco, CA, USA *231*, 1995, ID 196525
[3] Das, S. K., Choi, S. U. S., A Review of Heat Transfer in Nanofluids, in: *Advances in Heat Transfer*, (eds.: F. I. Thomas, P. H. James), Elsevier, Amsterdam, The Netherlands, 2009, pp. 81-197
[4] Haddad, Z., *et al.*, A Review on Natural Convective Heat Transfer of Nanofluids*,* R*enewable and Sustainable Energy* R*eviews*, *16* (2012), 7, pp. 5363-5378
[5] Haddad, Z., *et al.,* A Review on how the Researchers Prepare their Nanofluids*, International Journal of Thermal Sciences*, *76* (2014), Feb., pp. 168-189
[6] Wang, X.-Q., Mujumdar, A. S., Heat Transfer Characteristics of Nanofluids: a Review*, International Journal of Thermal Sciences*, *46* (2007), 1, pp. 1-19
[7] Murshed, S., K. *et al.,* Thermophysical and Electrokinetic Properties of Nanofluids – A Critical Review*, Applied Thermal Engineering, 28* (2008), 17-18, pp. 2109-2125
[8] Yu, W., *et al.,* Review and Comparison of Nanofluid Thermal Conductivity and Heat Transfer Enhancements*, Heat transfer engineering, 29* (2008), 5, pp. 432-460
[9] Kakac, S., Pramuanjaroenkij, A., Review of Convective Heat Transfer Enhancement with Nanofluids, *International Journal of Heat and Mass Transfer, 52* (2009), 13-14, pp. 3187-3196
[10] Ozerinc, S., *et al.,* Enhanced Thermal Conductivity of Nanofluids: A State-Of-The-Art Review*, Microfluidics and Nanofluidics, 8* (2010), 2, pp. 145-170
[11] Sarkar, J., A Critical Review on Convective Heat Transfer Correlations of Nanofluids*,* R*enewable and Sustainable Energy* R*eviews, 15* (2011), 6, pp. 3271-3277

[12] Sridhara, V., Satapathy, L. N., Al_2O_3-Based Nanofluids: A Review, *Nanoscale* R*esearch Letters, 6* (2011), 1, ID 456
[13] Nguyen, M. T., *et al.*, Natural Convection in a Non-Darcy Porous Cavity Filled with Cu-Water Nanofluid Using the Characteristic-Based Split Procedure in Finite-Element Method, *Numerical Heat Transfer, Part A: Applications: An International Journal of Computation and Methodology, 67* (2015), 2, pp. 224-247
[14] Aly, A. M., Ahmed, S. E., Double-Diffusive Natural Convective Flow of a Nanofluid Over a Vertical Cylinder, *Journal of Nanofluids, 5* (2016), 1, pp. 110-119
[15] Mansour, M. A., *et al.,* MHD Effects on Entropy Generation and Heat Transfer of Nanofluid Flows in Enclosures, Journal of *Nanofluids, 5* (2016), 4, pp. 595-605
[16] Aly, A. M., Raizah, Z. A., Double-Diffusive Natural Convection in an Enclosure Filled with Nanofluid Using ISPH Method, *Alexandria Engineering Journal, 55* (2016), 4, pp. 3037-3052
[17] Ahmed, S. E., *et al.,* Entropy Generation due to Mixed Convection over Vertical Permeable Cylinders Using Nanofluids, *Journal of King Saud University-Science, 31* (2017), 3, pp. 352-361
[18] Aly, A. M., Double-Diffusive Natural Convection in a Non-Darcy Porous Cavity Filled with Nanofluid under the Effects of Chemical Reaction, *Journal of Porous Media, 20* (2017), 2, pp. 111-126
[19] Nguyen, M. T., *et al.,* Effect of a Wavy Interface on the Natural Convection of a Nanofluid in a Cavity with a Partially Layered Porous Medium Using the ISPH Method, *Numerical Heat Transfer, Part A: Applications, 72* (2017), 1, pp. 68-88
[20] Aly, A. M., Raizah, Z. A. S., Mixed Convection in an Inclined Nanofluid Filled-Cavity Saturated with a Partially Layered Porous Medium, *Journal of Thermal Science and Engineering Applications, 11* (2019), 4, ID 041002
[21] Aly, A. M., *et al.,* Double-Diffusive Natural Convection in a Square Porous Cavity with Sinusoidal Distributions Side Walls Filled with a Nanofluid, *Journal of Porous Media 21* (2018), 2, pp. 101-122
[22] Sheikholeslami, M., Solidification of NEPCM under the Effect of Magnetic Field in a Porous Thermal Energy Storage Enclosure Using CuO Nanoparticles, *Journal of Molecular Liquids, 263* (2018), Aug., pp. 303-315
[23] Sheikholeslami, M., Numerical Simulation for Solidification in a LHTESS by Means of Nano-Enhanced PCM, *Journal of the Taiwan Institute of Chemical Engineers, 86* (2018), May, pp. 25-41
[24] Sheikholeslami, M., Influence of Magnetic Field on Al_2O_3-H_2O Nanofluid Forced Convection Heat Transfer in a Porous Lid Driven Cavity with Hot Sphere Obstacle by Means of LBM, *Journal of Molecular Liquids, 263* (2018), 1, pp. 472-488
[25] Li, Z., *et al.,* Investigation of Nanofluid Entropy Generation in a Heat Exchanger with Helical Twisted Tape, *Journal of Molecular Liquids, 266* (2018), Sept., pp. 797-805
[26] Sheikholeslami, M., Application of Darcy Law for Nanofluid Flow in a Porous Cavity under the Impact of Lorentz Forces, *Journal of Molecular Liquids, 266* (2018), Sept., pp. 495-503
[27] Rashad, A. M., *et al.,* Magnetic Field and Internal Heat Generation Effects on the Free Convection in a Rectangular Cavity Filled with a Porous Medium Saturated with Cu-Water Nanofluid, *International Journal of Heat and Mass Transfer, 104* (2017), Jan., pp. 878-889
[28] Shouguang, Y., *et al.,* Simulation of Flow Boiling of Nanofluid in Tube Based on Lattice Boltzmann Model, *Thermal Science, 23* (2019), 1, pp. 159-168
[29] Hemmat Esfe, M., *et al.,* Mixed Convection of Functionalized DWCNT-Water Nanofluid in Baffled Lid-Driven Cavities, *Thermal Science, 22, Part A* (2018), 6, pp. 2503-2514
[30] Bejjam, R. B., Kumar, K., Numerical Study on Heat Transfer Characteristics of Nanofluid Based Natural Circulation Loop, *Thermal Science, 22* (2018), 2, pp. 885-897
[31] Adjlout, L., *et al.*, Laminar Natural Convection in an Inclined Cavity with a Wavy Wall, *International Journal of Heat and Mass Transfer, 45* (2002), 10, pp. 2141-2152
[32] Misirlioglu, A., *et al.,* Free Convection in a Wavy Cavity Filled with a Porous Medium, *International Journal of Heat and Mass Transfer, 48* (2005), 9, pp. 1840-1850
[33] Das, P. K., Mahmud, S., Numerical Investigation of Natural Convection inside a Wavy Enclosure, *International Journal of Thermal Sciences, 42* (2003), 4, pp. 397-406
[34] Raizah, Z., *et al.,* Natural Convection Flow of a Power-Law Non-Newtonian Nanofluid in Inclined Open Shallow Cavities Filled with Porous Media, *International Journal of Mechanical Sciences, 140* (2018), May, pp. 376-393
[35] Aly, A. M., *et al.,* Mixed Convection in a Cavity Saturated with Wavy Layer Porous Medium: Entropy Generation, *Journal of Thermophysics and Heat Transfer, 32* (2018), 3, pp. 1-17

[36] Mahmud, S., *et al.*, Free Convection in an Enclosure with Vertical Wavy Walls, *International Journal of Thermal Sciences, 41,* (2002), 5, pp. 440-446
[37] Oztop, H. F., *et al.,* Natural Convection in Wavy Enclosures with Volumetric Heat Sources*, International Journal of Thermal Sciences, 50* (2011), 4, pp. 502-514
[38] Ahmed, S. E., *et al.*, Magnetohydrodynamic Mixed Thermo-Bioconvection in Porous Cavity Filled by Oxytactic Microorganisms, *Thermal Science, 22* (2018), 6B, pp. 2711-2721
[39] Nithyadevi, N., *et al.,* Numerical Study of MHD Mixed Convective Flow in a Lid-Driven Enclosure Filled with Nanofluid Saturated Porous Medium with Center Heater, *Thermal Science, 23* (2019), 3B, pp. 1861-1873
[40] Aron, S., *et al.*, *Convective Flow and Heat Transfer from Wavy Surfaces: Viscous Fluids, Porous Media, and Nanofluids*, CRC Press, Boka Raton, Fla, USA, 2016
[41] Sheremet, M. A., Pop, I.*,* Natural Convection in a Wavy Porous Cavity with Sinusoidal Temperature Distributions on both Side Walls Filled with a Nanofluid: Buongiorno's Mathematical Model*, Journal of Heat Transfer, 137* (2015), 7, ID 072601
[42] Sheremet, M. A., *et al.*, Free Convection in a Porous Wavy Cavity Filled with a Nanofluid Using Buongiorno's Mathematical Model with Thermal Dispersion Effect*, Applied Mathematics and Computation, 299* (2017), Apr., pp. 1-15
[43] Sheremet, M. A., *et al.,* MHD Natural Convection in an Inclined Wavy Cavity with Corner Heater Filled with a Nanofluid*, Journal of Magnetism and Magnetic Materials, 416* (2016), Oct., pp. 37-47
[44] Sheremet, M., *et al.,* Natural Convection of Nanofluid inside a Wavy Cavity with a Non-Uniform Heating: Entropy Generation Analysis*, International Journal of Numerical Methods for Heat & Fluid Flow, 27* (2017), 4, pp. 958-980
[45] Hamid, A. R, Alireza, S., MHD Natural Convection of Hybrid Nanofluid in an Open Wavy Cavity*,* R*esults in Physics, 9* (2018), June, pp. 440-455
[46] Sheikholeslami, M., *et al.*, Heat Transfer Behaviour of Nanoparticle Enhanced PCM Solidification through an Enclosure with V Shaped Fins*, International Journal of Heat and Mass Transfer, 130* (2019), Mar., pp. 1322-1342
[47] Sheikholeslami, M., Numerical Approach for MHD Al_2O_3-Water Nanofluid Transportation inside a Permeable Medium Using Innovative Computer Method*, Computer Methods in Applied Mechanics and Engineering*, *344* (2019), Feb., pp. 306-318
[48] Sheikholeslami, M., Finite Element Method for PCM Solidification in Existence of CuO Nanoparticles*, Journal of Molecular Liquids, 265* (2018), 1, pp. 347-355
[49] Sheikholeslami, M., Numerical Investigation of Nanofluid Free Convection under the Influence of Electric Field in a Porous Enclosure*, Journal of Molecular Liquids, 249* (2018), Jan., pp. 1212-1221
[50] Sheikholeslami, M., Numerical Investigation for CuO-H_2O Nanofluid Flow in a Porous Channel with Magnetic Field Using Mesoscopic Method*, Journal of Molecular Liquids, 249* (2018), Jan., pp. 739-746
[51] Sheikholeslami, M., Shehzad, S.*,* Numerical Analysis of Fe_3O_4-H_2O Nanofluid Flow in Permeable Media under the Effect of External Magnetic Source, *International Journal of Heat and Mass Transfer, 118* (2018), March, pp. 182-192
[52] Javaherdeh, K., *et al.,* Natural Convection of Nanofluid in a Wavy Cavity in the Presence of Magnetic Field on Variable Heat Surface Temperature*, Journal of Mechanical Science and Technology, 31* (2017), 4, pp. 1937-1945
[53] Chamkha, A. J., Ismael, M. A., Natural Convection in Differentially Heated Partially Porous Layered Cavities Filled with a Nanofluid*, Numerical Heat Transfer, Part A: Applications, 65* (2014), 11, pp. 1089-1113
[54] Chamkha, A. J., *et al.*, Mixed Convection in a Partially Layered Porous Cavity with an Inner Rotating Cylinder*, Numerical Heat Transfer, Part A: Applications, 69* (2016), 6, pp. 659-675
[55] Nguyen, M. T., *et al.,* ISPH Modeling of Natural Convection Heat Transfer with an Analytical Kernel Renormalization Factor*, Meccanica, 53* (2018), 9, pp. 2299-2318
[56] Ahmed, S. E., Raizah, Z. A. S.*,* Natural Convection Flow of Nanofluids in a Composite System with Variable-Porosity Media*, Journal of Thermophysics and Heat Transfer, 32* (2018), 2, pp. 495-502
[57] Cho, C.-C., Chen, C.-L., Natural Convection Heat Transfer Performance in Complex-Wavy-Wall Enclosed Cavity Filled with Nanofluid*, International Journal of Thermal Sciences, 60* (2012), Oct., pp. 255-263

Paper submitted: December 18, 2018
Paper revised: April 5, 2019
Paper accepted: April 11, 2019